ACS APPLIED MATERIALS & INTERFACES

Research Article

www.acsami.org

Sn Powder as Reducing Agents and SnO_2 Precursors for the Synthesis of SnO_2-Reduced Graphene Oxide Hybrid Nanoparticles

Mingxi Chen,[†] Congcong Zhang,[†] Lingzhi Li,[†] Yu Liu,*[,†,§] Xichuan Li,[†] Xiaoyang Xu,[†] Fengling Xia,[†] Wei Wang,[‡] and Jianping Gao*[,†,§]

[†]School of Science, [‡]School of Chemical Engineering, and [§]Collaborative Innovation Center of Chemical Science and Engineering, Tianjin University, Tianjin 300072, People's Republic of China

Supporting Information

ABSTRACT: A facile approach to prepare SnO_2/rGO (reduced graphene oxide) hybrid nanoparticles by a direct redox reaction between graphene oxide (GO) and tin powder was developed. Since no acid was used, it is an environmentally friendly green method. The SnO_2/rGO hybrid nanoparticles were characterized by ultraviolet−visible spectroscopy, Raman spectroscopy, thermogravimetric analysis, X-ray diffraction analysis, and X-ray photoelectron spectroscopy. The microstructure of the SnO_2/rGO was observed with scanning electron microscopy and transmission electron microscopy. The tin powder efficiently reduced GO to rGO, and the Sn was transformed to SnO_2 nanoparticles (~45 nm) that were evenly distributed on the rGO sheets. The SnO_2/rGO hybrid nanoparticles were then coated on an interdigital electrode to fabricate a humidity sensor, which have an especially good linear impedance response from 11% to 85% relative humidity.

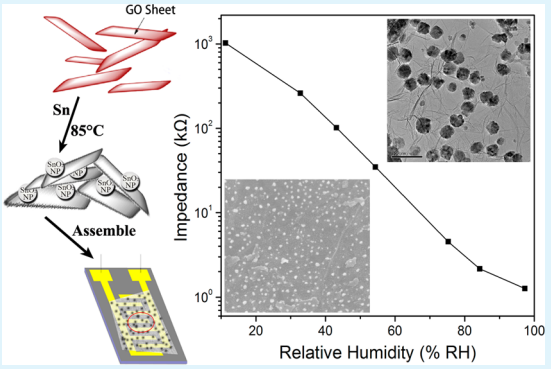

KEYWORDS: *SnO_2, nanoparticles, graphene, humidity sensor, reducing, environmentally friendly green method*

1. INTRODUCTION

Since it was first separated from graphite by Novoselov and coworkers in 2004, graphene has received tremendous attention in recent years.[1,2] Owing to its remarkable chemical,[3] mechanical,[4] and electronic properties,[5] it has great potential for applications in integrated circuits, field emitter transistors, lithium secondary batteries, transparent conductive electrodes in solar cells, biological and chemical sensors, and polymer composites.[6−8] Current methods to prepare graphene and graphene-like materials include the micromechanical exfoliation of graphite,[1] chemical vapor deposition,[9] epitaxial growth,[10] and the chemical reduction of graphene oxide (GO).[11−28] Although well-defined graphene can be produced using the first three methods, their low productivities make them unsuitable for mass production. The most promising and economically viable approach for the large-scale production of graphene-based materials is chemical reduction, in which cheap graphite powder is first oxidized using a strong oxidant to produce exfoliated GO and then the graphene oxide is reduced using chemical reduction or other routes.[11] Various chemicals have been used to reduce GO, such as hydrazine and its derivatives,[12,13] $NaBH_4$ and its derivatives,[14,15] hydriodic acid,[16] sulfur-containing compounds,[17] nascent hydrogen,[18−25] hydroxylamine,[26] ascorbic acid,[27] dextran,[28] and so on. Importantly, reduced graphene oxide (rGO) obtained by chemical reduction methods has unique properties, such as good electrical conductivity, it is dispersible in water, and it is versatile and easy to modify, which make it easy to process and use in applications, for example, fabricating sensors.[29,30]

During the last several decades, there has been a great deal of research and development directed toward the field of sensors. The function of a sensor is to provide physical, chemical, or biological information by converting this information directly into electrical signals.[31,32] There are many types of chemical sensors, including gas sensors, humidity sensors, ion sensors, drug sensors, and biosensors.[33−36] Humidity control is very important in many applications, industrial and agricultural production, and our daily lives. For example, in order to prevent fruits, vegetables, and other foodstuffs from rotting, they must be stored at a suitable humidity.

Many methods to detect humidity have been explored over the years, including wet and dry bulb thermometry, capacitive, resistive, and thermal conductive moisture detectors.[37] To further expand the measurement range, the sensitivity, the selectivity, and the chemical and thermal stability of humidity sensors, intensive efforts have been made to explore humidity sensors based on nanomaterials, such as carbon nanotubes,[38] metal oxide nanoparticles,[39] and nanowires.[40] Metal oxides, such as $MgCr_2O_4$-TiO_2, ZrO_2, and Al_2O_3, are mature nanomaterials that have been applied to humidity detection systems in industry.[37] SnO_2, a conductance-type semiconduc-

Received: October 1, 2013
Accepted: December 6, 2013
Published: December 6, 2013

tor, has been widely used to fabricate sensors,[41] and it has been extensively studied for gas sensors. For example, SnO_2 nanoribbons can detect hydrogen or ppm-level NO_2 at room temperature,[42,43] but it has seldom been applied in humidity sensors.[40] Generally, humidity sensors are based on the resistance of the material to the adsorption of water molecules.[33] Porous materials tend to make good humidity sensors since they have high specific surface areas, which improves adsorption and thus the performance of the humidity sensor.

Here, a simple method to prepare SnO_2/rGO hybrid nanoparticles for the fabrication of humidity sensors was developed. Sn powder was used to reduce GO, and SnO_2/rGO hybrid nanoparticles were formed. Unlike previous reductions of GO in the presence of metal powders, the GO was directly reduced by the Sn powder and no acid was needed. The reduction of GO with metal powders, such as Fe, Al, and Zn, is based on the hydrogen spillover mechanism.[18−21] Those metals react with acid to produce hydrogen that then reduces the GO. Therefore, large amounts of acids must be used, and the metal powder is usually in excess. RGO, as an excellent support, has a high specific surface area in addition to being chemically stable and corrosive resistant.[17] Therefore, SnO_2/rGO should be an outstanding material for building humidity sensors.

2. EXPERIMENTAL SECTION

2.1. Materials. Graphite was obtained from Qingdao Graphite Factory. Tin powder (the particle size is less than 75 μm; the melting point is 232 °C; the purity is more than 99.99%) was purchased from Aladdin Industrial Co. Potassium permanganate, sodium nitrate, concentrated sulfuric acid, 30% hydrogen peroxide, hydrochloric acid, ethanol, potassium carbonate, sodium chloride, potassium sulfate, potassium chloride, magnesium chloride, lithium chloride, and magnesium nitrate were all purchased from Tianjin Chemical Co. All the chemicals were analytical grade and used as received. Interdigital electrodes were purchased from Jinhua High-tech Co.

2.2. Preparation of GO. GO was prepared from purified natural graphite by a modified Hummer's method.[44] Briefly, concentrated H_2SO_4 was added to a 250 mL flask filled with graphite, followed by the addition of $NaNO_3$. Then, solid $KMnO_4$ was gradually added with stirring while the temperature of the mixture was kept below 20 °C. Next, the temperature was increased to 30 °C and excess distilled water was added to the mixture. Then the temperature was increased to 80 °C. Finally, 30% H_2O_2 was added until the color of the mixture changed to brilliant yellow. The mixture was filtered and washed several times with 5% aqueous HCl to remove metal ions and then washed with distilled water to remove the acid. The resulting filter cake was dried in air and then redispersed into water. Suspended GO sheets were obtained after ultrasonic treatment.

2.3. Preparation of SnO_2/rGO. First, 10 mL of GO suspension (0.5 mg/mL) and the desired amount of tin power were mixed in a beaker. Then, the solution was heated to 85 °C for 4 h with stirring, and the color of the solution gradually changed from brown to black. After reaction, the product was centrifuged and washed several times with deionized water before it was dried for 24 h at 60 °C in a vacuum oven to remove the water. The sample was stored in a desiccator. The weight ratio of Sn powder to GO was varied, and the resultant SnO_2/rGO samples are designated as SnO_2/rGO(1) and SnO_2/rGO(3) for Sn/GO ratios of 1 and 3, respectively.

2.4. Characterization. *2.4.1. Ultraviolet−Visible Spectroscopy Analysis.* The UV−vis absorption spectra of GO and rGO suspensions were recorded with a TU-1901 UV−vis spectrophotometer.

2.4.2. Scanning Electron Microscopy and Transmission Electron Microscopy Observation. The SnO_2/rGO hybrid nanoparticles were coated with gold using a sputter coater (Desk-II; Denton Vacuum), and then their morphologies were observed with a scanning electron microscopy (SEM) (S-4800, Thermo).

The sample for transmission electron microscopy (TEM) observation was prepared by placing drops of the diluted SnO_2/rGO aqueous suspension onto a carbon-coated copper grid, which was then dried under ambient conditions prior to being introduced into the TEM chamber. TEM observation and energy-dispersive X-ray spectroscopy (EDS) measurements were performed using a Philips Tecnai G2F20 microscope at 200 kV.

2.4.3. Raman Microscopy Analysis. Raman measurements were performed with an in Via high-resolution Raman microscope (RENISHAW, U.K.) in a backscattering configuration.

2.4.4. X-ray Diffraction Analysis. The X-ray diffraction (XRD) diagrams of the samples were measured using an X-ray diffractometer (BDX3300) with reference target: Cu Kα radiation (λ = 1.54 Å); voltage: 30 kV; and current: 30 mA. The samples were measured from 10° to 90° (2θ) with steps of 4° min^{-1}.

2.4.5. Thermogravimetric Analysis. The samples were first dried in a vacuum at 40 °C for 2 days before the thermogravimetric curves (TGA) were recorded with a Rigaku-TD-TDA analyzer at a heating rate of 10 °C/min.

2.4.6. X-ray Photoelectron Spectroscopy (XPS) Analysis. Elemental composition of the SnO_2/rGO was analyzed using an X-ray photoelectron spectrometer with a Mg Kα anode (PHI1600 ESCA System, PerkinElmer, US).

2.5. Assembly of Humidity Sensors. SnO_2/rGO (2 mg) and a few drops of ethanol were placed into a mortar and ground vigorously with a pestle to form a mixture. The mixture was smeared on an interdigital electrode that had been pretreated by shock cleaning in ethanol and acetone. The coated electrode was then dried for 12 h at 60 °C in a vacuum oven to obtain the SnO_2/rGO electrode.

According to Raoult's law, a saturated salt solution at a given temperature has its own specific humidity. Seven saturated salt solutions, LiCl, $MgCl_2$, K_2CO_3, $Mg(NO_3)_2$, NaCl, KCl, and K_2SO_4, were prepared to provide seven different relative humidity environments at 25 °C (Table S1, Supporting Information). To measure the change in impedance, the SnO_2/rGO electrode was connected to an LCR Bridge Meter (ZL5, Shanghai, China) and then placed over the saturated salt solution in a super thermostatic water bath (DF-101S, Yukang, China) at 25 °C. During the measurement, the whole system was hermetically sealed, as shown in Figure1.

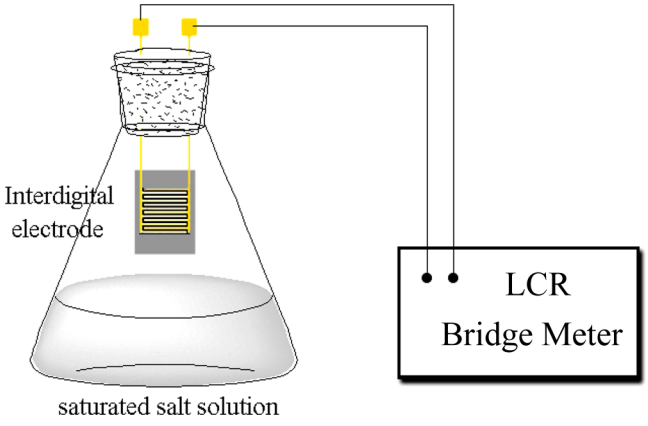

Figure 1. Schematic diagram of the setup for measuring impedance.

3. RESULTS AND DISCUSSION

3.1. Reaction between GO and the Sn Power. The GO was prepared in our laboratory by a modified Hummer's method.[45] It was centrifuged eight times to remove residual salts and acids, and then a stably dispersed GO aqueous suspension was prepared via ultrasonication. The aqueous suspensions were stable for several months, and no precipitation occurred. The GO nanosheets can also be suspended in *N*,*N*-dimethyl formamide and dimethyl sulfoxide,

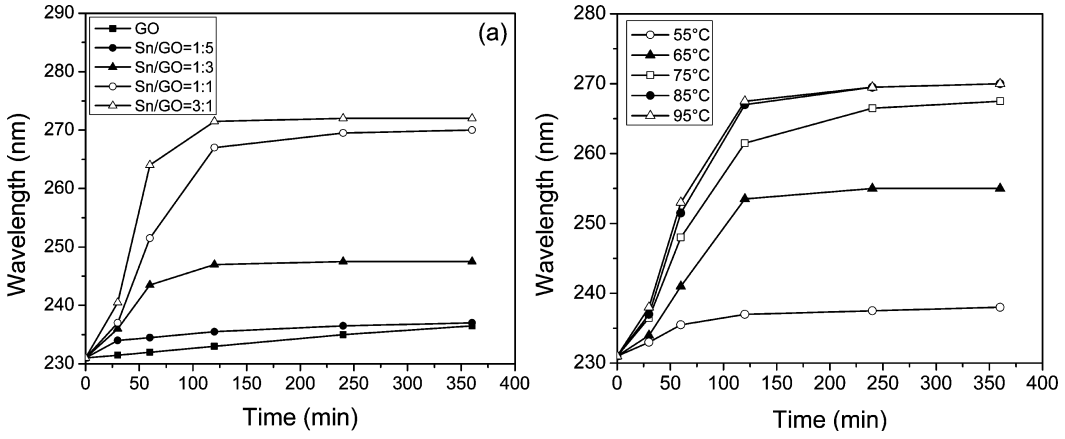

Figure 2. Effect of Sn/GO ratio (a) and reaction temperature (b) on the reduction of GO.

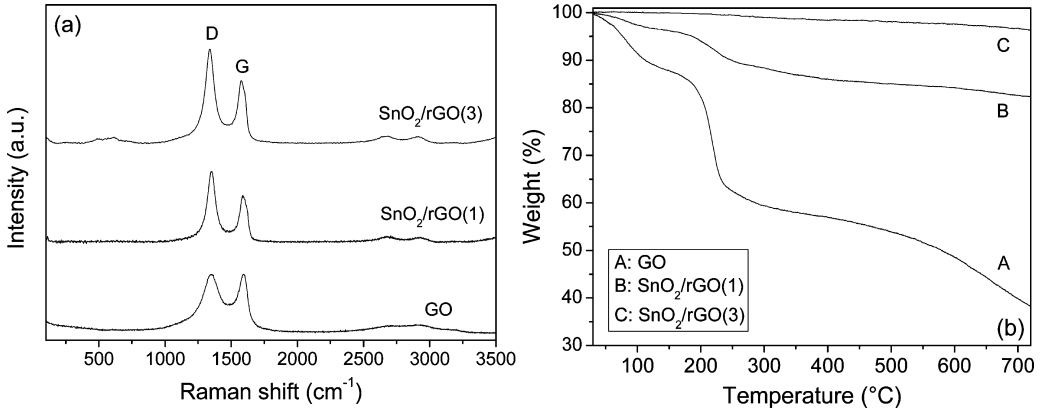

Figure 3. Raman spectra (a) and TGA curves (b) of GO, SnO_2/rGO(1), and SnO_2/rGO(3).

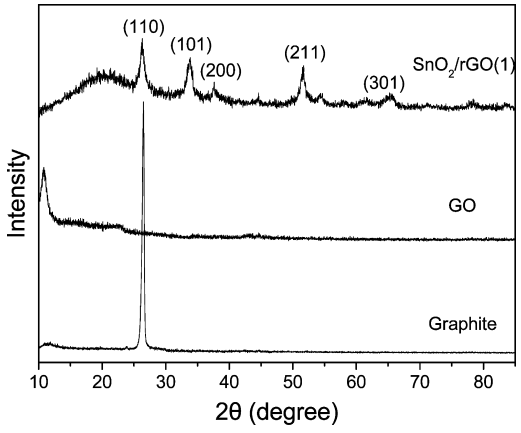

Figure 4. XRD diagrams of graphite, GO, and SnO_2/rGO(1).

implying that the GO nanosheets are both hydrophilic and thin enough to be suspended in numerous polar solvents, which has been further confirmed by UV−vis, TEM, XRD, and XPS. These stable GO aqueous suspensions are ideal raw materials for preparing stable suspensions of rGO or rGO hybrid nanoparticles.

To explore the transformation of GO during the reaction with the Sn powder, the pristine GO and the reaction products were characterized by UV−vis, Raman spectroscopy, TGA, and XPS. The product was first monitored with UV−vis spectroscopy, and the effects of reaction time and temperature are shown in Figure 2. The maximum GO absorption peak is at 231 nm, and when the reaction was performed in the absent of Sn powder, the peak position did not change much (Figure 2a). However, when the GO was reduced by tin powder for 4 h with Sn/GO ratios of 1:1 and 3:1, the peak red shifted to 270 and 265.5 nm, respectively. This phenomenon indicates that the electronic conjugation within the graphene nanosheets was restored and the GO was transformed to rGO.[43] When the mass ratio of Sn/GO was lower than 1:1, the GO was not reduced much.

Previous papers have reported that the reduction of GO occurs via the hydrogen spillover mechanism.[18−25] In these systems, hydrogen is the real reductant and not the metals. To produce sufficient hydrogen, excess metal and acids have to be used. For example, Barun et al. reported an approach to obtain rGO using Mg ribbons in an acidic solution.[25] The ratios of Mg/GO and Mg/HCl were 6.7 and 24.3, respectively. Although the reduction of GO was rapid, the C/O ratio in the rGO was only 3.95 and the post-treatment was relatively cumbersome because the excess acid and metal had to be removed. Using Fe-HCl as the reductant also required excess reagents and long reaction times (360 min) for the reduction of GO.[18] In this work, tin powder and GO were the only reactants, so it is believed that the tin powder is the reducing agent for the GO reduction rather than nascent hydrogen. Thus, this reaction does not produce acid pollution.

The effect of different temperatures on the reaction was also investigated, and the results are shown in Figure 2b. To obtain the good degree of reduction, the reducing temperature must be over 85 °C. Thus, the optimal reaction conditions are a Sn/

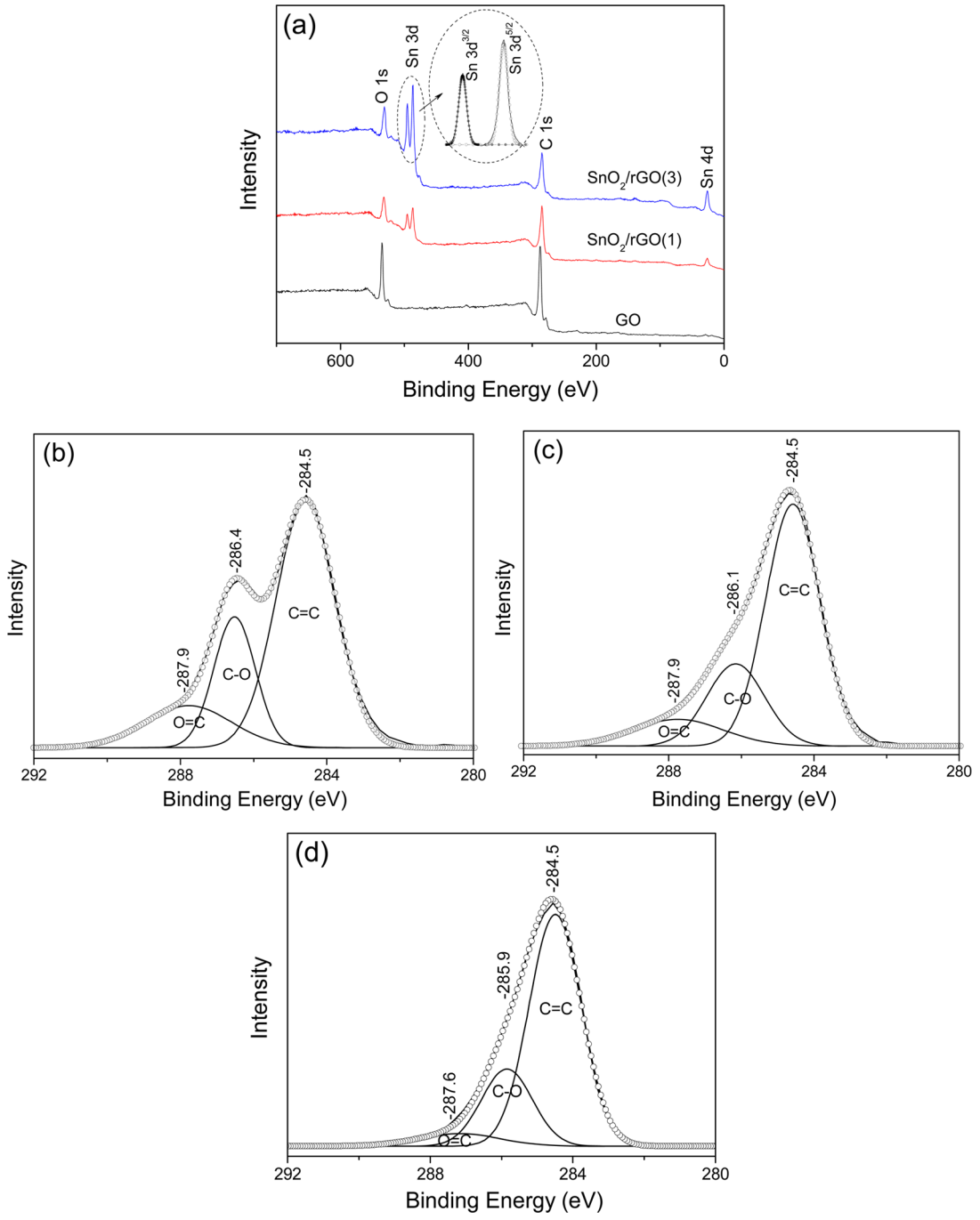

Figure 5. XPS spectra of GO, SnO_2/rGO(1), and SnO_2/rGO(3). The inset is the curve fit for the Sn 3d peak of SnO_2/rGO(3) (a); the curve fit for C 1s of GO (b); the curve fit for C 1s of SnO_2/rGO(1) (c); and the curve fit for C 1s of SnO_2/rGO(3) (d).

GO ratio of 3:1, a reaction temperature of 85 °C, and a reaction time of 4 h.

Raman spectroscopy is widely used to analyze carbon materials since it can provide information about defect density and structure, disorder, and doping levels. Generally, the Raman spectrum of graphene is characterized by two main features, the G mode arising from the first-order scattering of the E_{2g} phonons of the sp^2 C atoms (usually observed at ~1575 cm^{-1}) and the D mode due to the breathing mode of κ-point phonons with A_{1g} symmetry (at ~1350 cm^{-1}). Changes in the relative intensities of the D and G bands (D/G) indicate the changes in the electronic conjugation state of the GO during reduction. The Raman spectra of GO, SnO_2/rGO (1), and SnO_2/rGO (3) are shown in Figure 3a. The D/G ratio of rGO increased from 0.99 to 1.21 and 1.46. The increase in the D/G ratio suggests that sp^2 domains were formed and that GO was reduced during the reaction.[46]

TGA was performed to analyze the thermal stability of the sample, and the results are shown in Figure 3b. The GO shows two main weight losses. The first rapid weight loss (~15%) was at temperatures up to 100 °C and can be attributed to the removal of water molecules absorbed on the GO surface. The second weight loss (~25%) between 200 and 250 °C is due to decomposition of the oxygen-containing functional groups.[46] In comparison, the weight losses of SnO_2/rGO(1) and SnO_2/rGO(3) at 230 °C were only 4.1% and 1.2%, respectively. This

Table 1. Percentage of Different Bonds in GO, SnO_2/rGO(1), and SnO_2/rGO(3)

sample	analysis				
	carbon	oxygen[a]	tin		C/O ratio
GO	75.2	24.8	0		2.9
	C=C	C−O	C=O		
	57.9	29.9	12.2		
	carbon	oxygen[a]	tin	oxygen[b]	C/O ratio
SnO_2/rGO(1)	77	18.9	4.1	10.7	7.2
	C=C	C−O	C=O		
	68.8	21.8	9.4		
	carbon	oxygen[a]	tin	oxygen[b]	C/O ratio
SnO_2/rGO(3)	61.7	27.0	11.3	4.4	14.0
	C=C	C−O	C=O		
	73.2	19.9	6.9		

[a]Oxygen in SnO_2/rGO. [b]Oxygen in rGO.

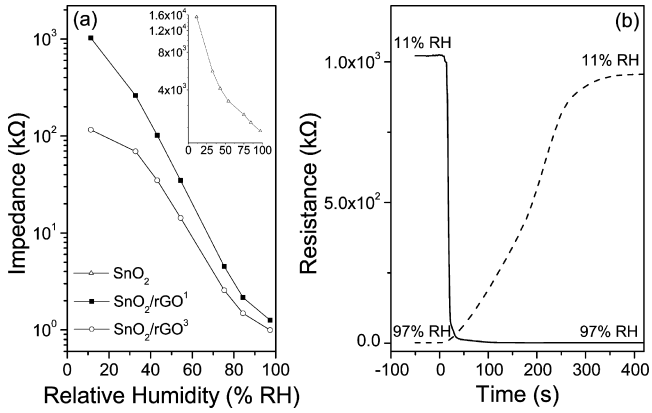

Figure 7. Impedance of SnO_2, SnO_2/rGO(1), and SnO_2/rGO(3) thin film humidity sensors (a). Response and recovery curves of the SnO_2/rGO(1) sensor (b).

clearly indicates that efficient deoxygenation can be achieved by using tin power and that increasing the SnO_2/GO ratio increases the extent of the GO reduction.

XRD is an effective method to explore the crystallinity of materials. The XRD patterns of graphite, GO, and the SnO_2/rGO(1) are shown in Figure 4. The GO spectrum has a characteristic peak at about 12.5° that represents an interlayer spacing of 0.74 nm. This is due to the oxygen-containing functional groups and the intercalation of water molecules. After GO was reduced, the amount of oxygen-containing functional groups decreased and the distance between layers was shortened. Therefore, the SnO_2/rGO(1) spectrum shows a weak broad peak at about 22° that is unlike the GO peak and the graphite peak at 26°. The peaks located at 26.61, 33.89, 37.95, 51.78, and 65.94° in the SnO_2/rGO(1) spectrum correspond to the tetragonal structure of SnO_2 (110), (101), (200), (211), and (301), respectively (JCPDS, card no. 41-1445). This indicates that the Sn transformed to SnO_2 nanocrystals during the redox reaction with GO and formed SnO_2/rGO hybrid nanoparticles.

The reaction products of the GO and tin powder were quantitatively characterized using X-ray photoelectron spectroscopy (XPS), and the results are shown in Figure 5 and Table 1. In the deconvoluted C 1s XPS spectrum of GO (Figure 5b), there are three peaks that are assigned to three types of carbon with different valences: nonoxygenated ring C (284.5 eV), carbon in C−O bonds (286.4 eV), and carbonyl C (287.9 eV).[44] However, in the C 1s spectrum of the rGO in SnO_2/rGO (Figure 5c,d), the amplitudes of the C−O and carbonyl C peaks decreased considerably, and that of the C=C peak increased greatly. This implies that, during the reduction, the oxygen functional groups were eliminated and the sp^2 domains were reestablished. Increasing the amount of the tin power decreased the amplitudes of both the C−O and carbonyl

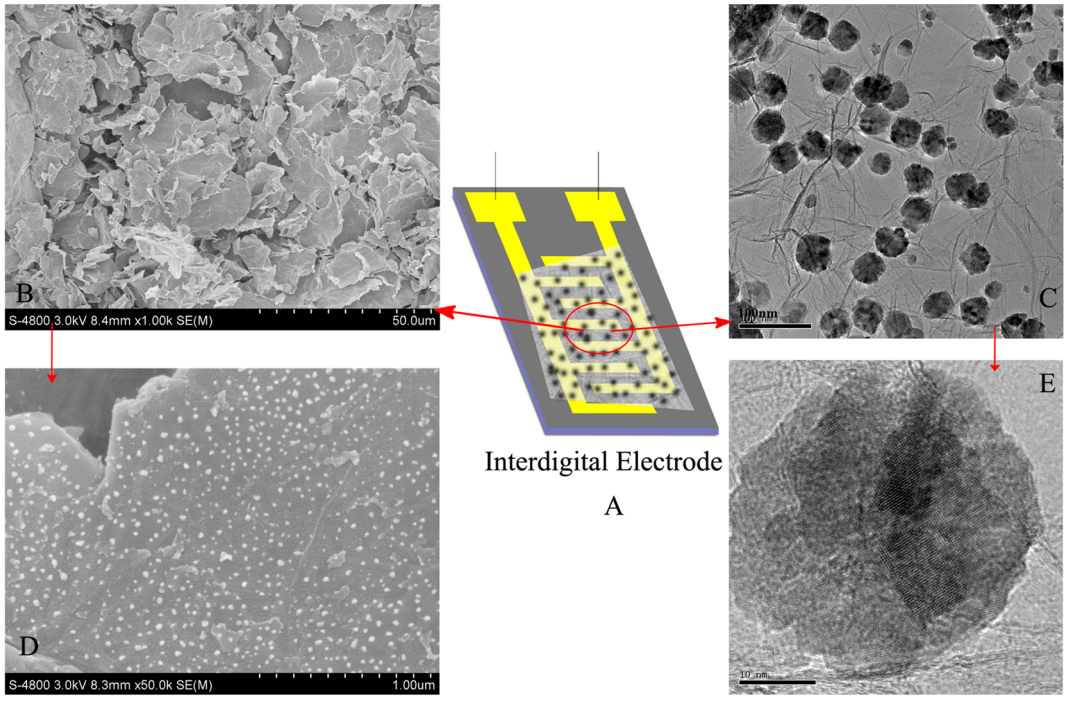

Figure 6. Schematic diagram of interdigital electrode coated with SnO_2/rGO(1) (A). SEM (B, D) and HRTEM (C, E) images of SnO_2/rGO(1).

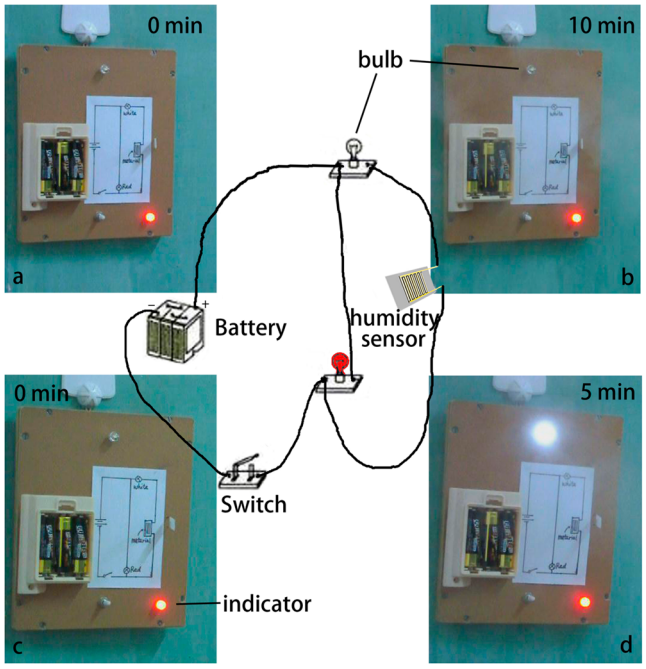

Figure 8. Screenshots from the video of interdigital electrodes: unloaded SnO2/rGO(1) (a, b) and loaded SnO2/rGO(1) (c, d).

C peaks. After the amount of oxygen in the SnO_2 is deducted from the total oxygen, the ratio of C/O in rGO increased from 2.9 to 7.2 for SnO_2/rGO(1) and to 14.0 for SnO_2/rGO(3). These are higher than that of rGO reduced by $NaBH_4$ (4.78).[47]

The reduction of GO by other metals (Al, Fe, Ni, Zn, and Mg) has also been reported, and those C/O ratios are shown in Table S2 (Supporting Information). With the exception of the rGO reduced by Al in an acidic environment, the C/O ratio of 14.0 for SnO_2/rGO(3) is the highest. However, all the GO in Table S2 were reduced via the hydrogen spillover mechanism, in which the reductant is hydrogen and not the metals. To produce sufficient hydrogen, a large amount of acid (or alkali) and metals must be used. This leads to troublesome post-treatments because the excess acid or base has to be removed. Therefore, in terms of water pollution, this is not a good method. The present approach needs no acid or base, so it is green and environmentally friendly.

XPS spectra are able to characterize not only the transformation of GO after the reaction but also the oxidation products of the tin. There are two peaks in the Sn 3d spectrum (Figure 5a). The one at 486.2 eV is attributed to Sn $3d_{5/2}$ of SnO_2, and the other at 495.5 eV is attributed to Sn $3d_{3/2}$ of SnO_2.[48] According to the peak area integration, the percentages of tin in the SnO_2/rGO(1) and SnO_2/rGO(3) are 4.1% and 11.3%, respectively, which indicates that almost all the tin powder was transformed to SnO_2 and loaded onto the rGO sheets. Therefore, the amount of SnO_2 loaded on the SnO_2/rGO can be adjusted by changing the initial Sn/GO ratio. Meanwhile, the mechanism is speculated that the standard electrode potential is the key factor in determining the redox reaction. The electrode potential of GO is +0.48 (relative to the standard hydrogen electrode),[49] and the standard potentials of the Sn oxidation reaction are given by the following:

$$Sn^{2+} + 2e^- \rightarrow Sn, \quad E^0 = -0.137$$

$$Sn^{4+} + 2e^- \rightarrow Sn^{2+}, \quad E^0 = 0.151$$

Therefore, the redox reaction can be carried out spontaneously, and Sn powders turn into tin ions. Because tin ions are apt to hydrolyze in the neutral, they transform to SnO_2 nanoparticles and load on the rGO. This method to prepare SnO_2/rGO hybrid nanoparticles is facile and has good stability and repeatability.

The prepared SnO_2/rGO hybrid nanoparticles were coated on the interdigital electrode to fabricate a humidity sensor (Figure 6A). The SEM and TEM photos of the SnO_2/rGO on the electrode are shown in Figure 6B–E. The rGO is layered (Figure 6B) due to the overlap of the rGO sheets during the SEM sample preparation. The rGO sheets are very thin and full of wrinkles (Figure 6C). The SnO_2 nanoparticles are round with diameters of about 45 nm. These SnO_2 nanoparticles are uniformly distributed on the rGO sheets (Figure 6C,D) and form SnO_2/rGO hybrid nanoparticles. In addition, the lattice fringes in the HRTEM image (Figure 6E; Figure S3, Supporting Information) indicate that the SnO_2 nanoparticle is made up of smaller SnO_2 crystals. The energy-dispersive X-ray spectroscopy (EDX) spectrum in Figure S1 (Supporting Information) shows only Sn on the rGO sheets, so this is a facile method to prepare high-purity SnO_2/rGO hybrid nanoparticles.

3.2. Application of SnO_2/rGO Hybrid Nanoparticles in Humidity Sensors. Figure 7a shows the humidity response curve of SnO_2, SnO_2/rGO(1), and SnO_2/rGO(3) at 25 °C. When the relative humidity changed from 11% to 97%, the impedances of SnO_2/rGO(1) and SnO_2/rGO(3) dropped by 3 and 2 orders of magnitude, respectively. The SnO_2/rGO(1) hybrid nanoparticles have an especially good linear impedance response from 11% to 85% relative humidity, which indicates that this material has good humidity sensing properties. Compared to humidity sensors prepared by similar materials reported,[40,49] this facile method provides an inexpensive material to assemble sensors, which is more valuable in the industrial production, and which has a wider linear range.[40,50] A few mechanisms have been proposed for explaining the surface conductivity change in the presence of water vapor.[40,51] In general, water molecules can be adsorbed by physisorption or hydrogen bonding. The SnO_2/rGO hybrids have an expanded measurement range compared to SnO_2 that may be related to the large surface area of the rGO, its extreme sensitivity toward changes in its local chemical environment, and the susceptibility of its electronic structure to interacting molecules.[36]

Further dynamic testing procedures were carried out, and the results are shown in Figure 7b. The response speed of the SnO_2/rGO(1) sensor was relatively fast, but the recovery rate was slow. In other words, it is relatively difficult for the adsorbed water molecules to desorb from the material. It is speculated that the potential energy of the material during desorption is greater than that during adsorption, and therefore, the water molecules need more time to desorb from the SnO_2/rGO(1). A simple video (in the Supporting Information) demonstrates the response of the SnO_2/rGO(1) humidity sensor to the change in humidity, and the video screenshots are shown in Figure 8. When a mist was sprayed onto the interdigital electrode without the SnO_2/rGO hybrid nanoparticles, the bulb did not light (Figure 8a,b); but when a mist was sprayed onto the interdigital electrode coated with SnO_2/rGO hybrid nanoparticles, the resistance of the SnO_2/rGO interdigital electrode became smaller and the bulb gradually brightens with exposure time (Figure 8c,d). The on/off state of the bulb is a signal of a change in humidity. This humidity

sensor can convert the change of humidity into a digital signal and could be applied to a control circuit.

4. CONCLUSIONS

A simple green method has been demonstrated to efficiently reduce GO with tin power without using any acid. The reaction between the tin powder and the GO produced SnO_2 nanoparticles with diameters of about 45 nm. These SnO_2 nanoparticles deposited on the GO sheets and formed SnO_2/rGO hybrid nanoparticles. SnO_2/rGO hybrid nanoparticles have good linear humidity sensing properties over a wide measurement range. The impedances span 3 orders of magnitude when the humidity changes from 11% to 85%. Therefore, the SnO_2/rGO hybrid nanoparticles obtained by this novel method show an exciting potential for use as sensors.

■ ASSOCIATED CONTENT

Supporting Information

Additional experimental data, including a video, TEM images, the EDX of SnO_2/rGO(1), and the C/O ratios of rGO prepared by using different metals. This material is available free of charge via the Internet at http://pubs.acs.org.

■ AUTHOR INFORMATION

Corresponding Authors

*Tel: +862227403475. Fax: (+86)22-2740-3475.
*E-mail: jianpinggaols@163.com (J.G.).

Notes

The authors declare no competing financial interest.

■ ACKNOWLEDGMENTS

This work was supported by the National Science Foundation of China (21074089, 21276181) and the Tianjin Municipal Science and Technology Commission, People's Republic of China (09JCZDJC23300).

■ REFERENCES

(1) Novoselov, K. S.; Geim, A. K.; Morozov, S. V.; Jiang, D.; Zhang, Y.; Dubonos, S. V.; Grigorieva, I. V.; Firsov, A. A. *Science* **2004**, *306*, 666−669.
(2) Geim, A. K.; Novoselov, K. S. *Nat. Mater.* **2007**, *6*, 183−191.
(3) Potts, J. R.; Dreyer, D. R.; Bielawski, C. W.; Ruoff, R. S. *Polymer* **2011**, *52*, 5−25.
(4) Dreyer, D. R.; Park, S.; Bielawski, C. W.; Ruoff, R. S. *Chem. Soc. Rev.* **2010**, *39*, 228−240.
(5) Allen, M. J.; Tung, V. C.; Kaner, R. B. *Chem. Rev.* **2010**, *110*, 132−145.
(6) Mao, S.; Pu, H. H.; Chen, J. H. *RSC Adv.* **2012**, *2*, 2643−2662.
(7) Zhu, Y. W.; Murali, S.; Cai, W. W.; Li, X. S.; Suk, J. W.; Potts, J. R.; Ruoff, R. S. *Adv. Mater.* **2010**, *22*, 3906−3924.
(8) Zhang, N.; Qiu, H.; Si, Y.; Wang, W.; Gao, J. *Carbon* **2011**, *49*, 827−837.
(9) Kim, K. S.; Zhao, Y.; Jang, H.; Lee, S. Y.; Kim, J. M.; Kim, K. S.; Ahn, J. H.; Kim, P.; Choi, J.; Hong, B. H. *Nature* **2009**, *457*, 706−710.
(10) Berger, C.; Song, Z.; Li, X.; Wu, X.; Brown, N.; Naud, C.; Mayou, D.; Li, T.; Hass, J.; Marchenkov, A. N.; Conrad, E. H.; First, P. N.; Heer, W. A. *Science* **2006**, *312*, 1191−1196.
(11) Seo, M.; Yoon, D.; Hwang, K. S.; Kang, J. W.; Kim, J. *Carbon* **2013**, *64*, 207−218.
(12) Stankovich, S.; Dikin, D. A.; Piner, R. D.; Kohlhaas, K. A.; Kleinhammes, A.; Jia, Y.; Wu, Y.; Nguyen, S. T.; Ruoff, R. S. *Carbon* **2007**, *45*, 1558−1565.
(13) Eda, G.; Fanchini, G.; Chhowalla, M. *Nat. Nanotechnol.* **2008**, *3*, 270−274.
(14) Si, Y.; Samulski, E. T. *Nano Lett.* **2008**, *8*, 1679−1682.
(15) Chua, C. K.; Pumera, M. *J. Mater. Chem. A* **2013**, *1*, 1892−1898.
(16) Moon, I. K.; Lee, J.; Ruoff, R. S.; Lee, H. *Nat. Commun.* **2010**, *1*, 73.
(17) Chen, M.; Zhang, C.; Li, X.; Zhang, L.; Ma, Y.; Zhang, L.; Xu, X.; Xia, F.; Wang, W.; Gao, J. *J. Mater. Chem. A* **2013**, *1*, 2869−2877.
(18) Fan, Z. J.; Kai, W.; Yan, J.; Wei, T.; Zhi, L. J.; Feng, J.; Ren, Y. M.; Song, L. P.; Wei, F. *ACS Nano* **2011**, *5*, 191−198.
(19) Fan, Z.; Wang, K.; Wei, T.; Yan, J.; Song, L.; Shao, B. *Carbon* **2010**, *48*, 1670−1692.
(20) Pham, V. H.; Pham, H. D.; Dang, T. T.; Hur, S. H.; Kim, E. J.; Kong, B. S.; Kima, S.; Chung, J. S. *J. Mater. Chem.* **2012**, *22*, 10530−10536.
(21) Liu, P.; Huang, Y.; Wang, L. *Mater. Lett.* **2013**, *91*, 125−128.
(22) Liu, Y.; Li, Y.; Zhong, M.; Yang, Y.; Wen, Y.; Wang, M. *J. Mater. Chem.* **2011**, *21*, 15449−15455.
(23) Yang, S.; Yue, W.; Huang, D.; Chen, C.; Lin, H.; Yang, X. *RSC Adv.* **2012**, *2*, 8827−8832.
(24) Krishna, R.; Titus, E.; Costa, L. C.; Menezes, J. C. J. M. D. S.; Correia, M. R. P.; Pinto, S.; Ventura, J.; Araujo, J. P.; Cavaleiro, J. A. S.; Gracio, J. J. A. *J. Mater. Chem.* **2012**, *22*, 10457−10459.
(25) Barman, B. K.; Mahanandia, P.; Nanda, K. K. *RSC Adv.* **2013**, *3*, 12621−12624.
(26) Zhou, X.; Zhang, J.; Wu, H.; Yang, H.; Zhang, J.; Guo, S. *J. Phys. Chem. C* **2011**, *115*, 11957−11961.
(27) Zhang, J.; Yang, H.; Shen, G.; Cheng, P.; Zhang, J.; Guo, S. *Chem. Commun.* **2010**, *46*, 1112−1114.
(28) Kim, Y. K.; Kim, M. H.; Min, D. H. *Chem. Commun.* **2011**, *47*, 3195−3197.
(29) Shi, Y.; Huang, W. T.; Luo, H. Q.; Li, N. B. *Chem. Commun.* **2011**, *47*, 4676−4678.
(30) Robinson, J. T.; Perkins, F. K.; Snow, E. S.; Wei, Z.; Sheehan, P. E. *Nano Lett.* **2008**, *8*, 3137−3140.
(31) Homola, J.; Yee, S. S.; Gauglitz, G. *Sensor Actuators, B* **1999**, *54*, 3−15.
(32) Adhikari, B.; Majumdar, S. *Prog. Polym. Sci.* **2004**, *29*, 699−766.
(33) Joo, S.; Brown, R. B. *Chem. Rev.* **2008**, *108*, 638−651.
(34) Yeo, T.L.; Sun, T.; Grattan, K.T.V. *Sensor Actuators, A* **2008**, *144*, 280−295.
(35) Meng, F.; Li, H.; Kong, L.; Liu, J.; Jin, Z.; Li, W.; Jia, Y.; Liu, J.; Huang, X. *Anal. Chim. Acta.* **2012**, *736*, 100−107.
(36) Wei, Y.; Gao, C.; Meng, F.; Li, H.; Wang, L.; Liu, J.; Huang, X. *J. Phys. Chem. C* **2012**, *116*, 1034−1041.
(37) Kulwicki, B. M. *J. Am. Chem. Soc.* **1991**, *74*, 697−708.
(38) Kauffman, D. R.; Star, A. *Angew. Chem., Int. Ed.* **2008**, *47*, 6550−6570.
(39) Su, P. G.; Wang, C. P. *Sensor Actuators, B* **2008**, *129*, 538−543.
(40) Kuang, Q.; Lao, C.; Wang, Z. L.; Xie, Z.; Zheng, L. *J. Am. Chem. Soc.* **2007**, *129*, 6070−6071.
(41) Kolmakov, A.; Zhang, X. Y.; Cheng, G. S.; Moskovits, M. *Adv. Mater.* **2003**, *15*, 997−1000.
(42) Comini, E.; Faglia, G.; Sberveglieri, G.; Pan, Z. W.; Wang, Z. L. *Appl. Phys. Lett.* **2002**, *81*, 1869−1871.
(43) Kind, L. H.; Messer, B.; Kim, F.; Yang, P. *Angew. Chem., Int. Ed.* **2002**, *41*, 2405−2408.
(44) Desiraju, G. R. *Acc. Chem. Res.* **2002**, *35*, 565−573.
(45) Guo, Y.; Sun, X.; Liu, Y.; Wang, W.; Qiu, H.; Gao, J. *Carbon* **2012**, *50*, 2513−2523.
(46) Pei, S.; Cheng, H. *Carbon* **2012**, *50*, 3210−3228.
(47) Shin, H. J.; Kim, K. K.; Benayad, A.; Yoon, S. M.; Park, H. K.; Jung, I. S.; Jin, M. H.; Jeong, H. K.; Kim, J. M.; Choi, J.Y.; Lee, Y. H. *Adv. Funct. Mater.* **2009**, *19*, 1987−1992.
(48) Grutsch, P. A.; Zeller, M. V.; Fehlner, T. P. *Inorg. Chem.* **1973**, *12*, 1431−1433.
(49) Chen, X.; Wu, G.; Chen, J.; Chen, X.; Xie, Z.; Wang, X. *J. Am. Chem. Soc.* **2011**, *133*, 3693−3695.
(50) Zappa, D.; Comini, E.; Sberveglieri, G. *Nanotechnology* **2013**, *24*, 444008.
(51) Henrich, V. A.; Cox, P. A. *The Surface Science of Metal Oxides*; University Press: Cambridge, U.K., 1994; p 312.